SAND2021-8702C

2021-01-1182

Catalyst-heating operation in a medium-duty diesel engine: operating strategy calibration, fuel reactivity, and fuel oxygen effects

Author, co-author (Do NOT enter this information. It will be pulled from participant tab in MyTechZone)

Affiliation (Do NOT enter this information. It will be pulled from participant tab in MyTechZone)

Abstract

Compliance with future ultra-low nitrogen oxide regulations with diesel engines requires the fastest possible heating of the exhaust aftertreatment system to its proper operating temperature upon cold starting. Late post injections are commonly integrated into catalyst-heating operating strategies. This experimental study provides insight into the complex interactions between the injection-strategy calibration and the tradeoffs between exhaust heat and pollutant emissions. Experiments are performed with certification diesel fuel and blends of diesel fuel with butylal and hexyl hexanoate. Further analyses of experimental data provide insight into fuel reactivity and oxygen content as potential enablers for improved catalyst-heating operation.

A statistical design-of-experiments approach is developed to investigate a wide range of injection strategy calibrations at three different intake dilution levels. Thermodynamic and exhaust emissions measurements are taken using a new medium-duty, single-cylinder research engine. Analysis of the results provides insight into the effects of exhaust gas recirculation, oxygenated fuel blends, and fuel reactivity on exhaust heat and pollutant emissions. Late-cycle heat release is an important factor in determining exhaust temperatures. Intake dilution and fuel properties certainly affect late-cycle heat release, but the methods applied in this work are not sufficient to reproduce or explain the mechanisms by which improved fuel cetane rating promotes operation with hotter exhaust and lower pollutant emissions.

Introduction

Modern diesel exhaust aftertreatment systems effectively reduce pollutant emissions, but only when the catalysts are operating above their respective light-off temperatures. One of the key objectives of the first minutes of diesel engine operation is therefore the rapid heating of the diesel oxidation catalyst and SCR catalyst to their proper operating temperatures. Both the temperature and mass flow of the engine exhaust play an important role in delivering thermal energy to the catalysts. In the absence of storage effects, pollutants formed in the combustion chamber are untreated and therefore emitted from the tailpipe until the catalysts are active. Compliance with upcoming ultra-low nitrogen oxide (NOx) emissions regulations (see, for example, [1]) requires effective exhaust heating strategies that quickly achieve light-off of the oxidation and SCR catalysts while maintaining pollutant emissions levels that do not exceed maximum allowable limits.

Catalyst-heating operation involves complex multiple-injection strategies with one or more late post injections that serve to increase exhaust temperatures [2, 3]. Modern common-rail fuel injection systems provide flexible control of the timing and quantity of each of these injections, which leads to a very large parameter space. Injection strategy calibrations that achieve high exhaust temperatures have been reported to result in higher fuel consumption, although measures such as cylinder deactivation or a mechanically driven turbocharger may offset some of these penalties over a drive cycle [4]. The tradeoffs that exist between engine calibration parameters, exhaust heat, and pollutant emissions during catalyst-heating operation and the mechanisms responsible for them have not been extensively documented.

Current understanding of how fuel properties influence catalyst-heating operation is insufficient to provide clear guidance on ideal fuel properties. Increased fuel cetane rating has been reported to enable improved catalyst-heating operation strategies [2], but the literature does not provide a satisfactory explanation of how more reactive fuels enable injection strategy calibrations with greater exhaust heat, lower pollutant emissions, or some combination of the two. Oxygenated biofuels can potentially reduce the net carbon footprint of diesel engines, and they are observed to affect the chemo-physical properties of diesel fuel in multiple ways [5]. However, the cumulative effects of these property changes on catalyst-heating operation have not been well characterized.

This paper presents an experimental study of engine calibrations intended to heat cold catalysts in a single-cylinder, medium-duty diesel research engine. An experimental approach based on statistical experiment design is developed and applied to a five-injection strategy at three different intake dilution levels. Precise thermodynamic analyses are applied to provide insight into heat-release behavior. The first objective of this work is to describe the tradeoffs that result between thermodynamic performance, exhaust enthalpy, and pollutant emissions. Next, the effects of oxygenated fuel blends on catalyst-heating operation are characterized. Finally, the effects of fuel reactivity on heat-release and emissions are isolated by blending diesel fuel with a cetane improver.

Methodology

Engine and catalyst-heating operation

The engine used in this work is a newly constructed, single-cylinder, medium-duty diesel research engine. The design of its dedicated four-valve cylinder head is based on that of the Ford 6.7L diesel engine [6]. The piston/rod assembly and fuel injector are production parts; the bore and stroke are identical to that of the production engine. The engine cradle is attached to a custom belt-driven Lanchester balancing box that compensates both first- and second-order oscillation forces. Engine speed is regulated with a 50-horsepower DC dynamometer. Pertinent data for the engine are given in Table 1; the engine and its auxiliary systems are shown in Figure 1.

Table 1: Engine and injector specifications

Bore	99 mm
Stroke	108 mm
Displacement volume	0.8315 L
Compression ratio	16.14:1 (estimated according to method in [7])
Valves	4
Fuel injector	8-hole piezo
Maximum speed (limited by balancing box design)	2000 rpm

Lubricating oil pressure is supplied to the crankshaft, camshaft, cam followers, rocker arms, and piston cooling jet by a five-stage dry sump pump driven by an electric motor. An industrial air compressor located above the lab provides pressurized air and an automatic pressure regulator combined with a calibrated critical flow orifice enables control of the intake air mass flow rate. Exhaust gas recirculation (EGR) is simulated with a mixture of air, nitrogen (N_2), and carbon dioxide (CO_2) designed to mimic the heat capacity and density of a real mixture of intake air and recirculated exhaust gas. The mass flow rates of the nitrogen and CO_2 are controlled with automatic pressure regulators and calibrated orifices. The temperature of the intake mixture is controlled with a 20 kW electric heater and band-heaters wrapped around the intake system (not shown in Figure 1). Pressurized fuel flows through a Coriolis mass flow meter on its way to an air-driven high-pressure pump. An additional pressure regulator (not shown in Figure 1) maintains the proper back pressure on the fuel injector return line. The fuel returned from the fuel injector and from the rail pressure control valve pass through a heat exchanger before being re-introduced upstream of the high-pressure pump and downstream of the Coriolis meter, so that only the fuel being consumed by the engine is measured. A custom-built system controls both the air pressure and rail pressure control valve. Nitrogen is used to dilute and cool the exhaust gases before they enter the exhaust surge tank. The mass flow of nitrogen is controlled with an automatic pressure regulator and a calibrated Venturi nozzle, and in this work its primary function is to reduce fouling of the exhaust emission analyzers. Exhaust backpressure is controlled with a cable-actuated exhaust throttle. Unburned hydrocarbons (UHCs), carbon monoxide (CO), and NO_x are measured with a flame ionization detector, non-dispersive infrared detector, and chemiluminescence detector, respectively.

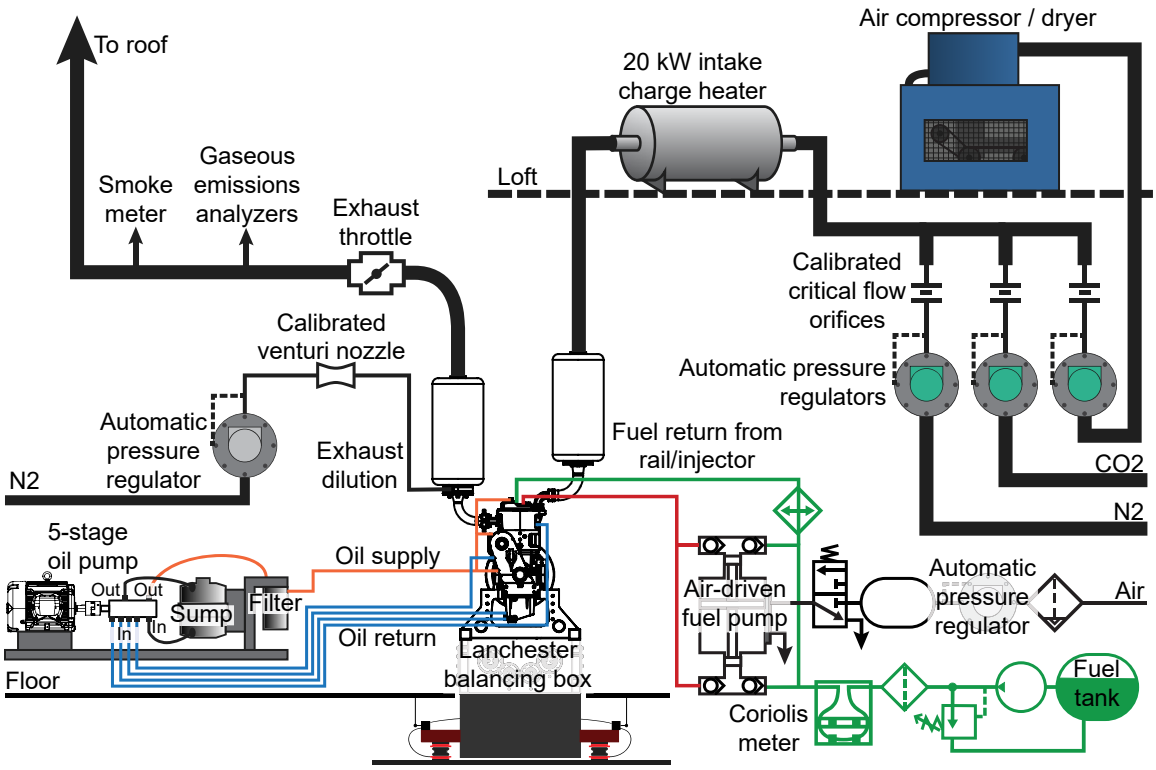

Figure 1: Simplified sketch of the medium-duty diesel combustion research lab at Sandia National Laboratories. Items are not drawn to scale and the coolant conditioning system is not shown.

An industrial crank angle encoder is installed on the engine crankshaft and has a resolution of 1/4 crank angle degrees (CAD). The engine control computer utilizes both rising and falling edges of both of the encoder's quadrature signals so the resolution of the engine controller is 1/16 CAD. A linear variable differential transformer (LVDT) is used to measure piston position and a least-squares fit of LVDT data with the known piston position function is used to phase the encoder's Z-pulse with TDC of the engine's crank. The maximum phasing error is estimated to be on the order of 0.1 CAD. Cylinder pressure is measured with a piezoelectric transducer mounted in a glow plug adapter and digitized every 0.25 CAD with a resolution of 16 bits. The output of a piezoresistive absolute pressure transducer installed in the intake runner is also measured and used to peg the cylinder pressure over a window near bottom-dead center, when both the intake pressure and cylinder pressure traces are relatively flat.

The operating point studied in this work has been chosen to represent catalyst-heating operation during the early portion of the cold start phase, when the engine hardware is relatively cold, and the engine load is relatively low. The variables and parameters associated with this operating point are summarized in Table 2. The variations in injection schedule calibrations are described below, but the main injection duration is adjusted to maintain the load for every injection strategy calibration and fuel. Thus, the total fueling amount changes throughout the experiment, although the intake mass flow rate is held constant. To maintain a constant EGR rate, the intake composition would need to be adjusted dynamically for each injection strategy calibration and fuel. Instead, the intake compositions are computed using a representative fuel flow rate and held constant for each simulated EGR rate. All references to EGR rates in this work correspond to these fixed intake compositions for the sake of convenience. Intake charge temperature is held constant regardless of EGR rate; this represents cooling of the exhaust gases by the cold EGR system components so that beneficial heating of the intake charge does not occur.

While these operating conditions result in a well-controlled and repeatable experiment, there are several key differences between this engine operation and catalyst-heating operation in a real multi-cylinder engine. In a real engine, the recirculated exhaust gases would contain species such as UHCs, CO, and NOx that could influence the ignition and combustion. This influence has the potential to build a feedback loop such that the exhaust products of one cycle would influence the combustion behavior of some number of subsequent cycles. These effects are not considered in this work. Next, catalyst-heating operation is inherently transient as the engine is warming up. In this work, coolant and oil temperatures are maintained at the lowest possible levels to preserve thermal boundary conditions. The complex five-injection strategy employed in this work results in significant pressure dynamics in the rail and the metal pipe that supplies fuel to the injector from the rail. These effects could be even more complex in a multi-cylinder engine, although model-based controls can compensate for these effects. Unfortunately, this technology is not available for the single cylinder engine used in this work. While offline measurements of injection quantities could be used to precisely control the mass of each injection, this would be practically impossible given the way in which engine load is controlled, the sensitivity of post injection quantities to the main quantity, and the large number of injection strategy calibrations studied in this work. Instead, injection energizing durations are determined by measuring injection quantities

with a hydraulic injection analyzer for the baseline condition, energizing durations are varied. More details of this methodology are provided below.

Table 2: Baseline engine operating condition

Coolant temperature	35°C		
Intake temperature	35°C		
Engine speed	1200 min^{-1}		
$IMEP_n$	3.25 ± 0.1 bar		
Intake flow rate	7.5 g/s		
Intake pressure (not controlled)	90-92 kPa		
Simulated EGR rate	5%	15%	30%
Intake [O_2]	20.557%	19.515%	17.428%
Intake [CO_2]	0.379%	1.269%	3.053%
Exhaust back pressure	128 kPa		
Exhaust dilution flow rate	10 g/s		
Rail pressure	700 bar		
Injection strategy	2 pilots, 1 main, 2 posts		

Fuels

A portion of this work has been funded by the U.S. Department of Energy's Co-Optimization of Fuels and Engines program. Within this program, a set of bio-blendstocks with properties well suited for mixing-controlled compression ignition has been identified [5]. Two of these blendstocks have been selected for the current work based partially on commercial availability and cost. Dibutoxymethane, or butylal (BA), is chosen because of its relatively high cetane number. Hexyl hexanoate (HH) is chosen for its similar oxygen content to that of BA and relatively low cetane number. Both of these oxygenated compounds are splash blended with the certification diesel fuel (CD) at 25 vol%. The properties of the baseline fuel and the two oxy-blends are given in Table 3.

To isolate the effects of reactivity from oxygen content and the thermophysical properties of the fuel, experiments are performed with certification diesel fuel that has been doped with di-tert-butyl peroxide (DTBP) at levels of 0.1 vol%, 0.2 vol%, 0.3 vol%, and 0.4 vol% to dramatically increase its reactivity with very small changes to its composition. While the cetane numbers of these mixtures have not been measured and are likely impossible to predict a priori [12], analysis of the results indicates that no doping level can result in heat release traces that match those of the more reactive BA25 blend over the range of EGR rates.

Table 3: Properties of the certification diesel and biofuel blends.

Property	Certification Diesel (CD)	BA25 blend	HH25 blend
Fuel oxygen ratio Ω_f [10]	0%	1.5%	1.3%
H/C ratio	1.812	1.896	1.854
O/C ratio	0	0.045	0.037
Density* (BA/HH data from [11])	0.8689 kg/m³	0.8415 kg/m³	0.8500 kg/m³
CN* (BA/HH data from [11])	46.0	52.0	44.6
Lower heating value* (BA/HH data from [11])	42.93 MJ/kg	40.8 MJ/kg	40.7 MJ/kg

*Density, cetane number, and lower heating value have been measured for the certification diesel but are estimated assuming ideal mixing for the fuel blends.

Experimental design and procedures

Because the five-injection strategy utilized in this work creates a very large parameter space, a systematic approach is necessary to maintain a reasonable experimental effort and study a relevant portion of the range of operation. To this end, a space-filling statistical experimental design is employed. Specifically, a nearly orthogonal/balanced design based on the work of MacCalman is developed [8, 9]. The experimental parameters and the ranges over which they are allowed to vary have been chosen based on discussions with technical experts at Ford Motor Company and are shown in Table 4. Injection timings are given in terms of the start of energizing (SOE) in crank angle degrees after top dead center (CAD ATDC). Dwells between injection events are given in microseconds and the injection durations are listed as duration of energizing (DOE). The approximate total mass of the pilots is reported based on offline measurements with a hydraulic injection analyzer. Note that these are only estimates, in large part because the back pressure in the hydraulic analyzer cannot be made to match the back pressure in the engine over the range of injections. The pilot mass is nearly evenly divided between both pilots.

Table 4: Injection parameters. Variables chosen for the statistical experiment design are shown in bold type.

EGR rate; discrete variable	5%, 15%, 30% (see Table 2)
SOE(1st pilot); continuous variable	[-24.4, -16.4] CAD ATDC
Dwell between 1st and 2nd pilot (fixed)	1102 µs
Total pilot mass (approximate)	3.5 mg
Dwell between 2nd pilot and main (fixed)	1151 µs
DOE of main (continuous variable)	Varied to maintain load
Dwell between main and 1st post; continuous variable	[1250, 3264] µs
DOE of 1st post + 2nd post (fixed)	599 µs
Ratio of DOE(1st post) / DOE(1st post + 2nd post); continuous variable	[32.6, 67.4]%
Dwell between 1st and 2nd post; continuous variable	[417, 1806] µs

A total of 71 parameter combinations have been chosen for the final space-filling design. The resulting injector energizing calibrations are depicted in Figure 2. For each of the certification diesel fuel (CD), the butylal blend (BA25), and the hexyl hexanoate blend (HH25), the following procedure is followed to produce results that are as repeatable as possible:

1. For the given EGR rate, the engine is fired using the calibration that produces the hottest exhaust for 20 minutes (this was determined through previous experiments).
2. The desired injection strategy calibration for the given EGR rate is loaded into the engine control program. The main injection duration is adjusted to achieve the target load within approximately 20 seconds.
3. After three minutes of engine operation, a measurement of 100 cycles of cylinder pressure data are taken, along with a 30-second average of emissions, temperature, and fuel flow rate data.
4. Steps 2 and 3 are repeated for each injection strategy calibration for the given EGR rate in the order shown in Figure 2.
5. The engine is stopped. Steps 1-4 are repeated for each of the three EGR rates.

After this procedure has been executed for a given fuel, the fuel system is flushed with n-heptane, purged with nitrogen, and filled with the next fuel. The lubricating oil and oil filter are changed along with the fuel to minimize the possibility of cross-contamination with different fuels.

A reduced set of injection strategy calibrations is employed for the fuel reactivity variation. The following calibrations are chosen for each EGR rate:

1. A baseline calibration that can be used to assess repeatability
2. The calibration resulting in minimum CO emissions
3. The calibration resulting in maximum exhaust heat; this is also the calibration with the minimum NO_x emissions
4. The calibration resulting in minimum NO_x + UHC emissions

An exception is made for the 5% EGR rate: instead of the maximum-exhaust-heat calibration, a calibration point is chosen that is unexceptional in terms of every comparison metric. This set of calibrations is shown in Figure 3. A procedure similar to the one given above is followed for each of the diesel-DTBP blends.

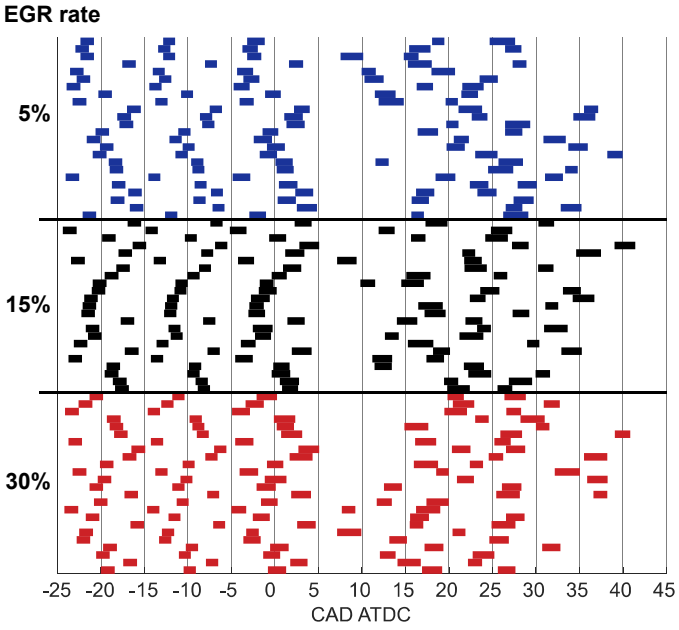

Figure 2: Injector energizing calibrations: each row corresponds to an injection strategy calibration and a distinct engine operating point. The calibrations are grouped by EGR rate but have not been sorted in any other way.

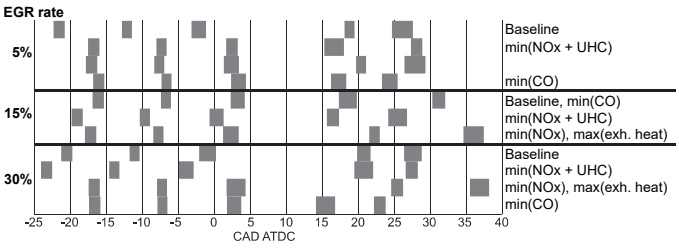

Figure 3: Injector energizing calibrations for the fuel reactivity study.

Data processing

Heat-release analyses are performed using ensemble-averaged cylinder pressure measurements together with the intake flow rate and composition, as well as the fueling rate. The rate of heat-release is computed from the first law of thermodynamics as follows:

$$\frac{dQ_{HR}}{d\theta} = P\frac{dV}{d\theta} + \frac{1}{\gamma-1}\left(P\frac{dV}{d\theta} + V\frac{dP}{d\theta}\right) + \frac{dQ_{wall}}{d\theta} \quad (1)$$

P and $\frac{dP}{d\theta}$ are cylinder pressure and its derivative with respect to crank angle θ.

Each individual cylinder pressure trace is digitally filtered using a low-pass filter with a 3.5-kHz cutoff point (3 dB attenuation). P is the ensemble average of these filtered pressure traces.

V and $\frac{dV}{d\theta}$ are cylinder volume and its derivative with respect to crank angle θ.

γ is the ratio of specific heats. It is computed as a function of temperature and modeled mixture composition. The composition of the intake charge is known, as are the products of complete, stoichiometric combustion for a given fuel composition. The mixture composition is comprised of fresh charge (including the simulated EGR components) and products of complete combustion. The amount of combustion products is computed using the mass fraction burned: the integrated heat release normalized by the fuel energy supplied. Fuel vapor and products of incomplete combustion are not considered for the calculation of γ.

$\frac{dQ_{wall}}{d\theta}$ is the rate of wall heat loss, given by

$$\frac{dQ_{wall}}{d\theta} = \frac{h_{Woschni}A_{cyl}}{n}\left(T_{cyl} - T_{wall}\right) \quad (2)$$

A_{cyl} is the instantaneous surface area of the combustion chamber, T_{cyl} is the bulk gas temperature as computed with the ideal gas law, and T_{wall} is the wall temperature, assumed to be 40°C. n is the engine speed, and $h_{Woschni}$ is the convective heat transfer coefficient as computed by the Woschni correlation [13, 14]:

$$h_{Woschni} = C_m B^{-0.2} P^{0.8} {T_{cyl}}^{-0.546}\left[C_1 v_{mp} + C_2(P - P_{mot})\right]^{0.8} \quad (3)$$

C_m is a tuning parameter, B is the bore diameter given in Table 1, and v_{mp} is the mean piston speed. P_{mot} is the motored cylinder pressure, computed in a manner similar to that described in [15]. C_1 is the scale factor for the velocity in a motored engine, given by:

$$C_1 = a + b\left(\frac{\pi B R_s}{2S}\right) \quad (4)$$

a is 6.18 during the intake and exhaust strokes, and 2.28 during the compression and expansion strokes [14]. b is 0.417 during the intake and exhaust strokes, and 0.308 during the compression and expansion strokes [14]. R_s is the swirl ratio, assumed to be 1.7 [6]. S is the stroke given in Table 1. C_2 is a second tuning parameter that scales the combustion-induced velocity.

C_m and C_2 are calibrated similarly to what is described by Dernotte et al. [15]. C_m is adjusted so that the integrated *apparent* heat release (that is, assuming $dQ_{wall} = 0$) is equal to the integrated wall heat loss for a motored cylinder pressure trace. For this operating condition, C_m is computed to be 5.64. C_2 is computed for a fired trace so that the integrated heat release at exhaust valve opening is equal to the amount of fuel energy released as heat: $m_f Q_{LHV} \eta_{comb}$, where m_f is the measured fuel mass per cycle, Q_{LHV} is the fuel's lower heating value as given by Table 3, and η_{comb} is the combustion efficiency calculated from the exhaust emissions measurements (see Equation 6). C_2 may be computed so that this condition is met when averaged over all measured operating points for a given fuel or for any specific operating point. When computed as an average over all operating points for a given fuel, C_2 is 0.0038, and in fact this value is the same for each of the fuels shown in Table 3. For the ensemble-averaged data shown in this work, this value of C_2 has been used. Where results of individual operating points are shown, C_2 has been calibrated for each fuel for that operating point.

In this work, thermal efficiency is defined as the ratio of net indicated work to the fuel energy released (not the fuel energy delivered):

$$\eta_{th} = \frac{W_i}{m_{fuel}\, Q_{LHV}\, \eta_{comb}} \quad (5)$$

W_i is the boundary work done over the full cycle.

Combustion efficiency is determined from the exhaust emissions measurements:

$$\eta_{comb} = 1 - \frac{\dot{m}_{exhaust}\left(y_{UHC}Q_{LHV} + y_{CO}Q_{LHV,CO}\right)}{\dot{m}_{fuel}Q_{LHV}} \quad (6)$$

y_{UHC} and y_{CO} are the mass fractions of unburned hydrocarbons (assumed to have the same heating value as the fuel) and CO, respectively. $\dot{m}_{exhaust}$ and $\dot{m}_{fuel}$ are the mass flow rates of exhaust and fuel, respectively. $Q_{LHV,CO}$ is the lower heating value of CO, 10.10 MJ/kg.

This way, the overall indicated efficiency is proportional to the product of thermal efficiency and combustion efficiency, such that both can be independently examined.

In addition to exhaust temperature, the flow of exhaust enthalpy is critical for increasing catalyst temperatures. It is normalized by the engine's displacement volume and expressed as follows:

$$\Phi_{ex} = \frac{c_{p,exh}\left(\dot{m_{air}} + \dot{m_{fuel}}\right)\Delta T}{V_d} \quad (7)$$

Φ_{ex} is called the exhaust heat flux and is expressed in kW/L. $c_{p,exh}$ is the specific heat of the exhaust gas, taken to be 1.25 kJ/kgK for the sake of simplicity (see Figure 4-17 in [14]). $\dot{m_{air}} + \dot{m_{fuel}}$ is the total mass flow rate of exhaust, computed as the sum of the flow rate of air that is not associated with the simulated EGR and the flow rate of fuel. Thus, the displacement of fresh air with EGR will reduce exhaust heat flux.

ΔT is defined as $T_{exh} - 20°C$

V_d is the displacement volume of the engine given in Table 1.

Finally, the degree of constant volume combustion is computed from the heat release trace to characterize the degree to which it represents

ideal, constant-volume combustion. Increasing the degree of constant volume combustion generally means that the heat release is taking place earlier during the expansion stroke and more work can be extracted from the gas in the cylinder. The calculation follows the work of Shudo and Nabetani [16]:

$$DCVC = \frac{1}{\eta_{Otto} Q_{HR}} \int \left(1 - \left(\frac{V_d + V_c}{V}\right)^{1-\gamma} \frac{dQ_{HR}}{d\theta}\right) d\theta \qquad 8$$

V_c is the clearance volume and Q_{HR} is the integrated heat release evaluated at exhaust valve opening.

η_{Otto} is the Otto-cycle efficiency, which is simply computed with a constant value for γ of 1.33.

$$\eta_{Otto} = 1 - r_c^{1-\gamma} \qquad 9$$

r_c is the compression ratio, given in Table 1.

Results and Discussion

Combustion efficiency, net-indicated specific fuel consumption (ISFCn), and thermal efficiency are plotted against the degree of constant volume combustion for the entirety of experiments performed with certification diesel fuel in Figure 4.

EGR and injection strategy effects

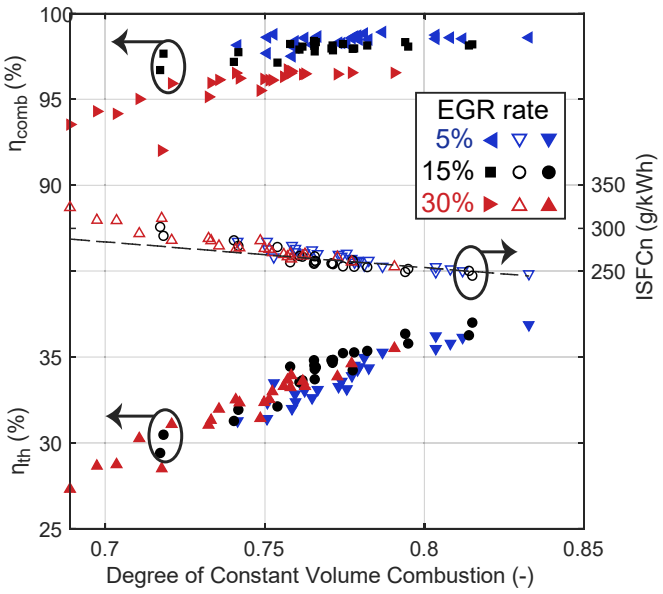

Figure 4: η_{comb}, ISFCn, and Thermal Efficiency plotted against the degree of constant volume combustion. The dashed line is only shown for reference and is not fitted to any data.

The variety of injection strategy calibrations shown in Figure 2 results in a range of heat-release profiles and therefore in a range of values for the degree of constant volume combustion (DCVC). For calibrations that result in more retarded combustion phasing, DCVC and thermal efficiency are lower. As a result, fuel consumption increases. At very low values of DCVC the combustion efficiency begins to decrease and the fuel required to meet the target load increases. This is evident in the departure from linear behavior of the fuel consumption. Higher EGR rates result in lower values of DCVC, which is consistent with slower combustion. It is also evident that increasing EGR has a negative effect on combustion efficiency: lower intake oxygen concentrations result in less complete combustion.

Exhaust temperature and heat flux are plotted against DCVC in Figure 5. As DCVC decreases, thermal efficiency decreases and less energy is extracted from the cylinder content, thus resulting in higher exhaust temperatures. Indeed, the hottest exhaust temperatures are achieved with the highest EGR rates and it appears the primary reason is the slower combustion possible with elevated EGR rates. The inherent tradeoff between efficiency and exhaust temperature shown in Figure 4 and Figure 5 appears to be a fundamental limitation. Despite the hottest exhaust temperatures occurring at the highest EGR rates, the highest exhaust heat flux values occur with the lowest EGR rates. As EGR displaces fresh air in the intake, less mass flows through the catalysts which has a negative effect on exhaust heat flux (see equation 6).

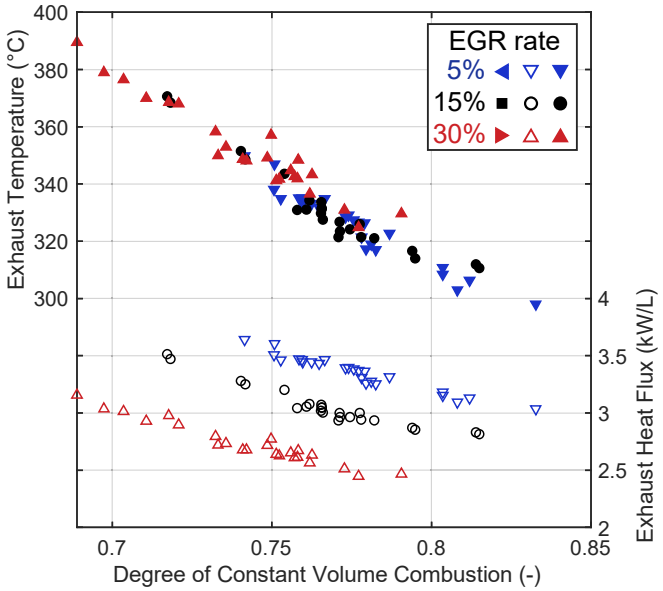

Figure 5: Exhaust temperature and heat flux plotted against the degree of constant volume combustion. Achieving the hottest exhaust temperature may not be the same as achieving the highest exhaust heat flux.

The injection strategy calibrations that result in the coldest and hottest exhaust for each EGR rate are shown in Figure 6. The similarities amongst the three coldest calibrations and amongst the three hottest calibrations are remarkable. For the hottest calibrations, the first post injection starts between 20 and 25 CAD ATDC and the commanded duration is shorter than that of the second post, which starts near 35 CAD ATDC. However, based on the limited number of calibrations studied in this work it is not possible to conclude that the three hottest calibrations shown result in the absolute maximum achievable exhaust temperature for each EGR rate.

An examination of bulk gas temperatures provides further insights into the in-cylinder phenomena responsible for the behavior shown in Figure 5. Bulk-gas temperature is plotted against crank angle in Figure 7, along with the measured exhaust temperatures. The

temperatures at the end of the heat-release calculation at 120 CAD ATDC follow the same trend as the measured exhaust temperatures: the relative ordering is properly calculated. The earlier combustion phasing associated with the coldest-exhaust calibrations results in peak temperatures that are higher than for the hottest-exhaust calibrations. Peak bulk-gas temperatures correlate very poorly with exhaust temperatures: the highest bulk gas temperature occurs with 5% EGR, which results in the lowest exhaust temperature. Rather, exhaust temperatures are more strongly correlated with the phasing of the temperature maximum associated with the combustion of the post mixture, or the temperature measured later in the cycle. It is clear that the ordering of temperatures by EGR rate is established in the later phases of combustion: after 30 CAD ATDC for the coldest calibrations and after 60 CAD ATDC for the hottest calibrations.

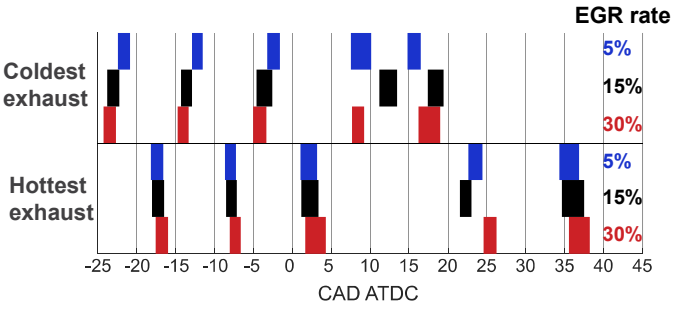

Figure 6: Injector energizing calibrations resulting in the lowest exhaust temperatures (blue) and the hottest exhaust temperatures (red) for each EGR rate.

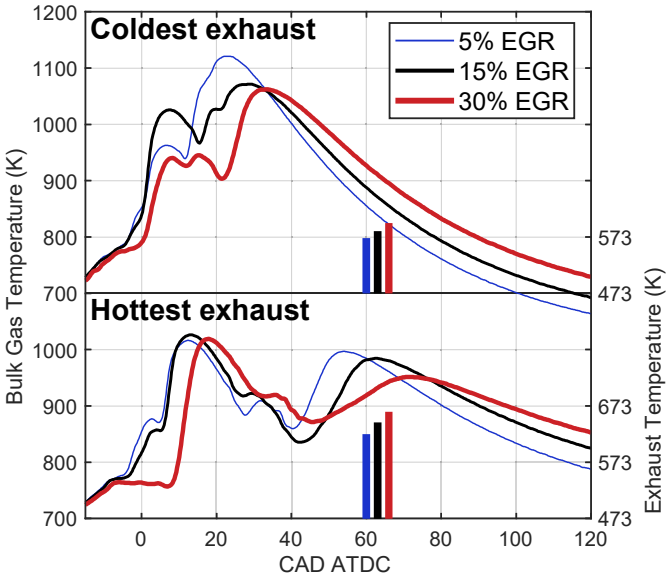

Figure 7: Bulk gas temperature plotted against crank angle for the coldest-exhaust calibrations (top) and hottest-exhaust calibrations (bottom). Measured exhaust temperatures are shown with bar plots but the horizontal locations of the bars have no significance.

The effects of EGR rate on heat-release are shown in Figure 8 for the hottest-exhaust calibrations at 5% and 30% EGR. While the injection strategy calibrations for the two EGR rates shown are not identical, the effect of intake dilution on heat-release rates appears to be considerably larger than what could be attributed to differences in injection phasing and duration alone. The lower oxygen concentrations associated with higher EGR levels likely suppress the heat release of the pilot injections and delay the high-temperature ignition process. Similarly, the heat-release associated with the post injections is suppressed and spread over a wider crank angle range. The main injection timing is also later for the 30% EGR case than for the 5% EGR case. In the absence of other effects, a later main injection timing would tend to reduce efficiency and increase the fueling requirement. The combination of later pilot-main injection phasing, suppressed heat release rates, and lower combustion efficiency (see Figure 1) act to increase the fueling required for the 30% EGR case: the total amount of heat released is nearly 7% higher than for the 5% EGR case. However, it isn't until approximately 70 CAD ATDC that the cumulative heat release for the 30% EGR case exceeds that of the 5% EGR case later in the cycle: a significant fraction of the total heat-release occurs at very late crank angles, which has significant implications for exhaust temperature (see Figure 7).

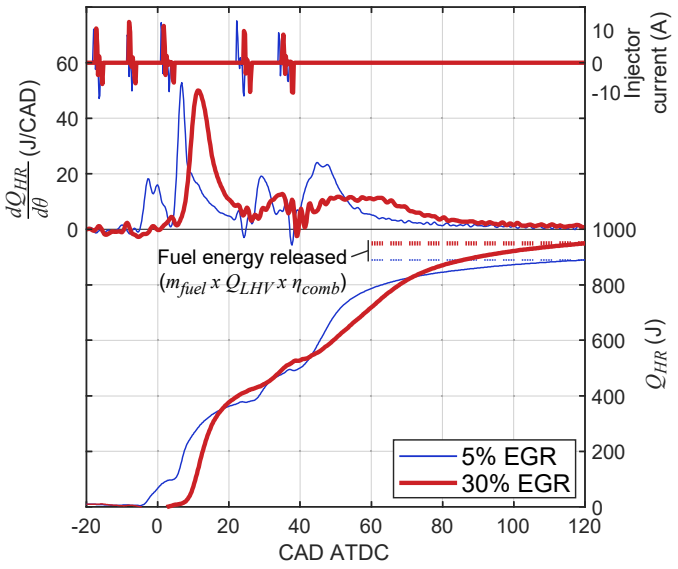

Figure 8: Injector current, heat-release rate, and cumulative heat release plotted against crank angle for the hottest-exhaust calibrations at 5% EGR (dashed blue) and 30% EGR (solid red). The horizontal lines on the right indicate the total fuel energy released for each case.

The gaseous pollutant emissions for the variation of EGR rate and injection strategy calibration are shown in Figure 9. In general, NO_x emissions depend more strongly on EGR rate than on injection strategy calibration. However, for a given EGR rate, NO_x emissions tend to decrease as the degree of constant volume combustion decreases. The EGR effect is consistent with hotter in-cylinder temperatures due to faster, earlier heat release at the lowest intake dilution levels (see Figure 7 and Figure 8), as well as an increase in local combustion temperatures. The dependency on injection strategy calibration is consistent with the data shown in Figure 7: for the calibrations with hot exhaust, bulk gas temperatures spend a comparatively short time above 1000 K than they do for the coldest-exhaust calibrations.

The unburned hydrocarbon emissions data collapse to a large extent when plotted against DCVC. UHC emissions increase as combustion phasing is retarded and as EGR rate increases. While the sources of

UHC emissions are not well understood for catalyst-heating operation, several factors likely contribute to the observed behavior. Figure 8 demonstrates that pilot heat release is incomplete even for the lowest EGR level: a total pilot quantity of 3.5 mg (see Table 4) corresponds to approximately 150 mJ with the certification diesel fuel. At 5% EGR, the cumulative heat release associated with the combustion of the pilots is only approximately 100 mJ. The long ignition delays of the pilots likely result in mixtures that are leaner than the flammability limits of the fuel, such that the pilot fuel is not fully consumed before the high-temperature heat-release associated with the main injection begins. At 30% EGR, there isn't a high-temperature heat-release event that can be attributed to the pilot injections alone and the delay from the start of the first pilot to the start of high temperature heat-release is greater than 20 CAD. Thus, overmixing of the pilot fuel is likely exacerbated by EGR. As post injection timings are retarded, less time is available for complete oxidation of the fuel; lower intake oxygen concentrations will most certainly hinder this oxidation to a greater extent. On the other hand, the calibrations with the hottest exhaust tend to have the highest bulk-gas temperatures during the late stages of combustion (see Figure 7). These high temperatures would promote oxidation, but this effect is apparently not enough to overcome the effects of time and oxygen concentration so UHCs tend to increase as combustion phasing is retarded and intake oxygen concentration is decreased.

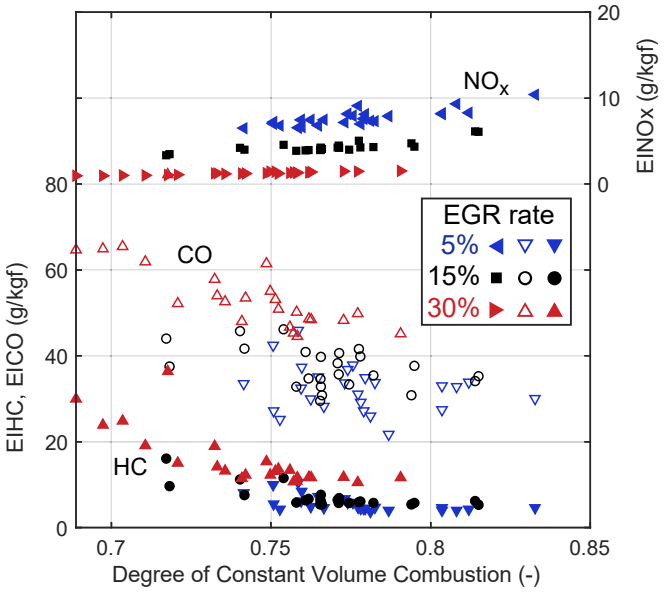

Figure 9: Emissions indices of NOx (top points), CO (middle points), and UHC (bottom points) plotted against the degree of constant volume combustion with EGR rate as a parameter.

Carbon monoxide emissions do not collapse well with DCVC, but are generally observed to increase as DCVC decreases. CO formation under these operating conditions is also not well understood. Rich mixtures necessarily result in CO emissions, but the extent to which lean mixtures do depends strongly on the evolution of local temperatures and equivalence ratios [17]. Given the previous discussion of long pilot/main ignition delays, rich pilot/main mixtures seem an unlikely source of CO emissions. Furthermore, smoke emissions that have been measured for some of the calibration points correlate poorly with CO emissions, which suggests that the rich mixtures responsible for soot formation are not the only source of CO. As with UHCs, later post injection timings leave less time for CO oxidation reactions to reach completion. The general increase in CO emissions as DCVC decreases is consistent with this phenomenon. Higher CO emissions levels are observed at higher EGR levels.

The data shown in Figure 4, Figure 5 and Figure 9 demonstrate the inherent tradeoffs in catalyst-heating operation. As combustion phasing is retarded to increase exhaust temperatures, NO_x emissions and efficiency decrease. EGR slows combustion reactions and therefore promotes even higher exhaust temperatures. The benefits in exhaust temperature come at the price of increased CO and UHC emissions, which degrade combustion efficiency. EGR effectively reduces NO_x emissions but results in a substantial penalty in exhaust mass flow and therefore exhaust heat flux.

If the amount of energy required to heat a catalyst to its light-off temperature is constant, then catalyst-heating operation may be expected to have a small effect on overall fuel consumption. Figure 4 and Figure 5 demonstrate a clear tradeoff between efficiency and exhaust heat: energy used to do work cannot be used to create hotter exhaust. Thus, more efficient calibrations would decrease the rate of fuel consumption. However, the associated low exhaust enthalpy would require a longer amount of time required for catalyst light-off, and earlier combustion phasing increases peak bulk-gas temperatures (Figure 7) and wall heat-loss rates. Conversely, less efficient calibrations with lower DCVC values would consume fuel at a higher rate but would achieve catalyst light-off in a shorter amount of time. The only possibilities to simultaneously reduce fuel consumption and improve catalyst heating performance are to reduce wall heat losses or to increase combustion efficiency. The critical need to meet NOx emissions standards means that the catalysts must reach their light-off temperatures in the shortest time possible, so efforts to improve combustion efficiency or reduce wall heat losses should be focused on calibrations with low values of DCVC and high exhaust temperatures.

Oxygenate blend effects

One of the first observations made in the study of oxygenate blends is that the fuel blend does not change the calibration required to achieve the hottest exhaust (although the main injection duration is adjusted to maintain load), and typically doesn't change the calibrations required to achieve minimum NO_x, CO, and UHC + NO_x emissions. It is unclear if this finding would remain if a larger number of calibrations were investigated.

Fuel effects on heat-release behavior are most pronounced for the 30% EGR cases. The injector current, heat-release rate, and cumulative heat-release are shown in Figure 10 for the hottest-exhaust calibration at 30% EGR. The more reactive BA25 blend maintains a degree of high-temperature pilot heat-release, whereas the CD and HH25 blend do not. The main heat-release is also enhanced by the more reactive BA25 blend: the heat release ramps up faster and reaches a higher peak value than for the other two fuels. Both the main and post heat-release events finish sooner with BA25 than with CD. Because BA25 burns earlier and more efficiently, less fuel energy is required to achieve the target load than for the other fuels. On the other hand, more fuel energy is required with HH25. This fuel energy is released after the time of peak heat-release for the main injection, which is when the cumulative heat-release curves for CD and HH25 diverge from one another. The differences in cumulative heat-release are nearly constant between 30 and 60 CAD ATDC, at which point fuel effects are again observed. Heat-release rates decline slightly sooner for the BA25 blend, followed closely by the HH25 blend. In contrast, heat-release continues

slightly later into the cycle with certification diesel; the cumulative heat-release for the CD case doesn't exceed that of the BA25 case until approximately 85 CAD ATDC. These differences have important implications for measured exhaust temperatures, but the competing effects of oxygen content, energy content, and reactivity make it difficult to discern which effects are most responsible for this behavior.

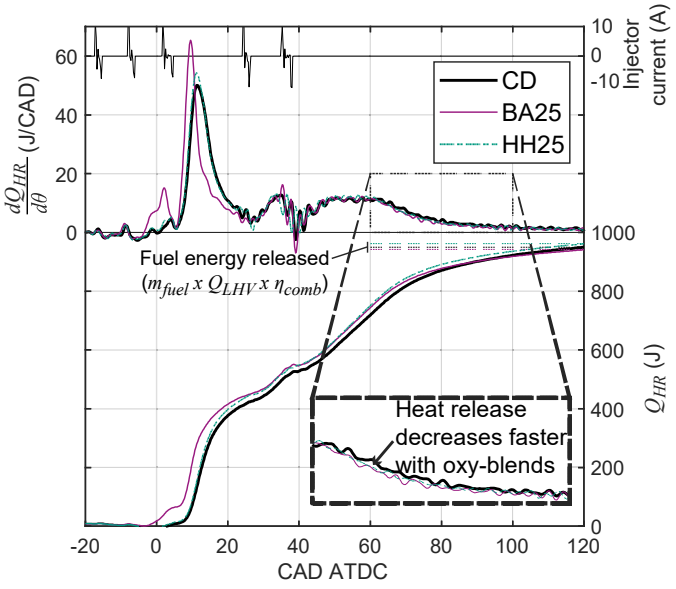

Figure 10: Injector current, heat-release rate, and cumulative heat release plotted against crank angle for the hottest-exhaust calibration, 30% EGR case. Certification diesel (CD): thick black line; butylal blend (BA25): thin purple line; hexyl hexanoate blend (HH25): dashed teal line. The horizontal lines on the right indicate the total fuel energy released.

Figure 11 shows heat-release analysis results for the third injection strategy calibration shown in Figure 3; the EGR rate is 5%. As with the 30% EGR case, the more reactive BA25 blend enhances pilot combustion, but to a lesser extent at 5% EGR. The high-temperature ignition of the pilot mixture is advanced and the corresponding peak heat-release rate is increased. The total amount of energy released by the pilot injections is higher than for the certification diesel and HH25 blend, even though the energy contained in the pilot injections is likely lower for the BA25 blend than for the CD fuel due to BA25's lower energy content and lower mass density than those of CD. In contrast to the 30% EGR case, the BA25 blend is associated with the lowest peak heat-release rate, although the decline in heat-release rate is again observed to occur soonest for the BA25 blend. The heat-release event associated with the second post injection is slightly advanced with BA25 compared to CD, but the same is not true for the HH25 blend, which results in an evolution of heat-release for the second post injection that is very similar to that of CD. The persistence of reactivity with the CD fuel late into the cycle is again observed, although this effect is considerably smaller than for the 30 % EGR case.

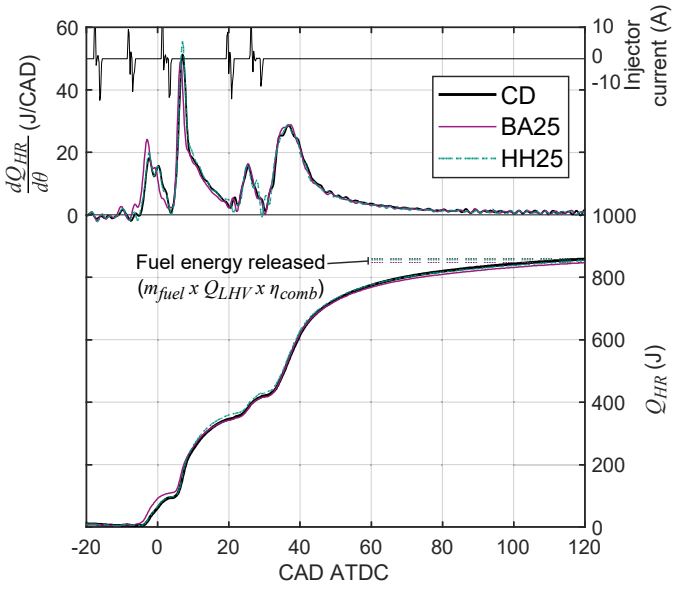

Figure 11: Injector current, heat-release rate, and cumulative heat release plotted against crank angle for a 5% EGR case. Certification diesel (CD): thick black line; butylal blend (BA25): thin purple line; hexyl hexanoate blend (HH25): dashed teal line. The horizontal lines on the right indicate the total fuel energy released.

A statistical analysis of the results of the oxygenate blend study provides a better understanding of how these effects tend to influence catalyst-heating performance. To achieve this, paired t-tests are performed to evaluate the hypothesis that the oxygenate blends have no effect on thermal efficiency, DCVC, cumulative wall heat loss, exhaust heat, exhaust mass flow, and exhaust temperature. These results are shown in Figure 12. For each plot, colored bars are shown to indicate the relative change between values measured for each oxygenate blend and compared to the values measured for CD. One of three alternative hypotheses are evaluated for each bar shown:

- "B" the oxygenate blend either decreases or increases the value of interest.
- "L" the oxygenate blend increases the value of interest.
- "R" the oxygenate blend decreases the value of interest.

For each bar, the p-value is shown. This value represents the probability that the observations would be made if the null hypothesis were true. P-values lower than the threshold value (α) of 0.05 are shown in **bold** type and indicate that the trend shown is statistically significant. P-values just above 0.05 are interpreted as limited evidence of the trends shown. Each bar is a one-dimensional heat-map of values to indicate the distribution of observed differences over all calibrations at a given EGR rate. The black dots represent the mean value of relative differences, and the horizontal error bars show one standard deviation of the relative differences in each direction from the mean.

A variety of factors determines the effects of the oxygenate fuel blends on thermodynamic performance of catalyst-heating operation. While no strong evidence exists that these fuels affect thermal efficiency, there is some limited evidence that BA25 improves thermal efficiency at 30% EGR. Two main factors are responsible for influencing thermal efficiency: the degree of constant volume combustion and wall heat loss. Evidence exists that both oxygenate blends result in more advanced heat release phasing (see Figure 10

and Figure 11), particularly for BA25 and for both blends at 30% EGR, although longer main injections are typically necessary to deliver the required fuel energy. Evidence is strong that both oxygenate blends tend to increase cumulative wall heat loss, even though this is not always the case with HH25. This is consistent with more advanced combustion phasing and the resulting higher bulk gas temperatures with the oxygenate blends.

While no evidence exists that HH25 affects exhaust enthalpy compared to CD, there is strong evidence that BA25 reduces exhaust enthalpy at 30% EGR. Here too, two competing factors explain this behavior. On the one hand, the lower energy content of the oxygenate blends results in higher fuel mass flows to maintain the target load. The statistical evidence of this effect is strong at each EGR rate and for both fuels. On the other hand, exhaust temperature is affected differently by these two oxygenated fuels. The HH25 blend does not have a statistically significant effect on exhaust temperature. However, evidence is strong that BA25 reduces exhaust temperatures; the relative decreases shown correspond to reductions in exhaust temperature that may exceed 10 K. It is not entirely clear why BA25 decreases exhaust temperatures to a much larger extent than HH25, but earlier heat release phasing (higher DCVC values) results in more work extraction and higher wall heat losses, and therefore in less available enthalpy out of the cylinder, and to the exhaust.

The statistical analysis of oxygenated fuel blend effects on pollutant emissions are summarized in Figure 13.

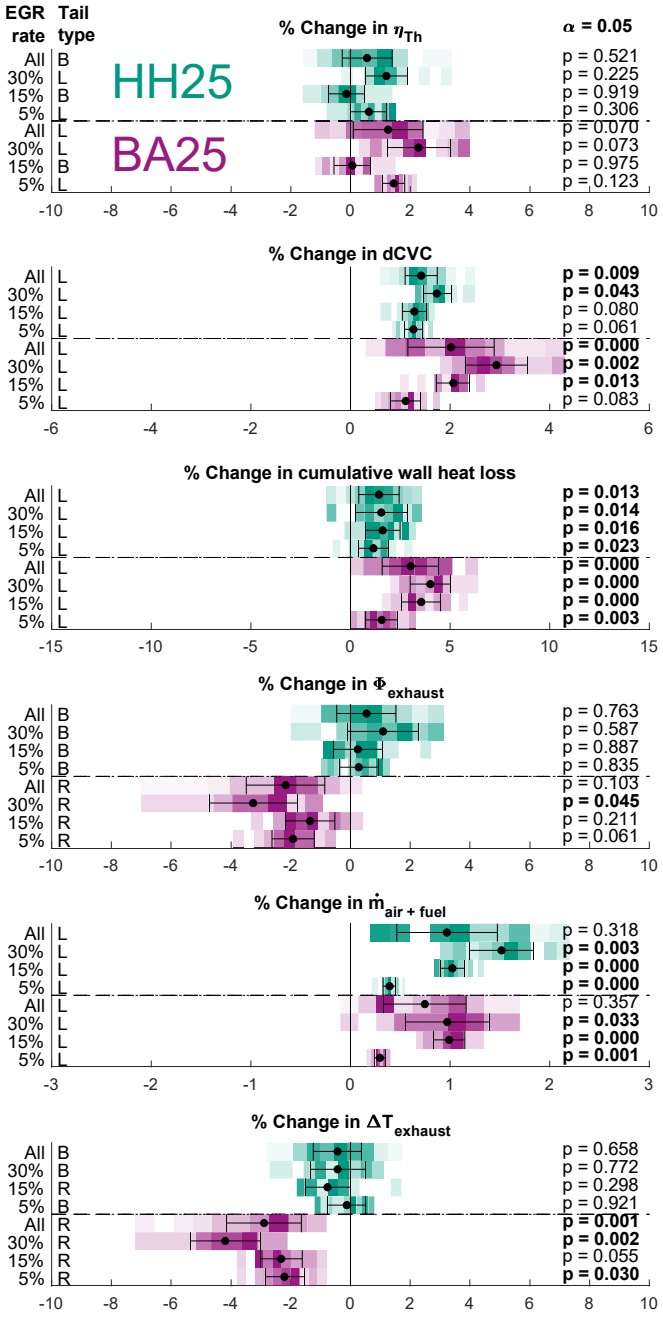

Figure 12: T-test evaluations of effects of oxygenate blends on thermodynamic performance. The plots show the changes in thermal efficiency, the degree of constant volume combustion, the cumulative wall heat loss, the exhaust heat flux, the flow of fresh air and fuel, and the difference between exhaust temperature and ambient temperature, relative to the values obtained with certification diesel. The colored bars are used to indicate the distribution of values for each EGR rate and overall for both HH25 (teal) and BA25 (purple). The black dots represent the mean value of the relative differences and the black lines indicate the standard deviation of the relative differences.

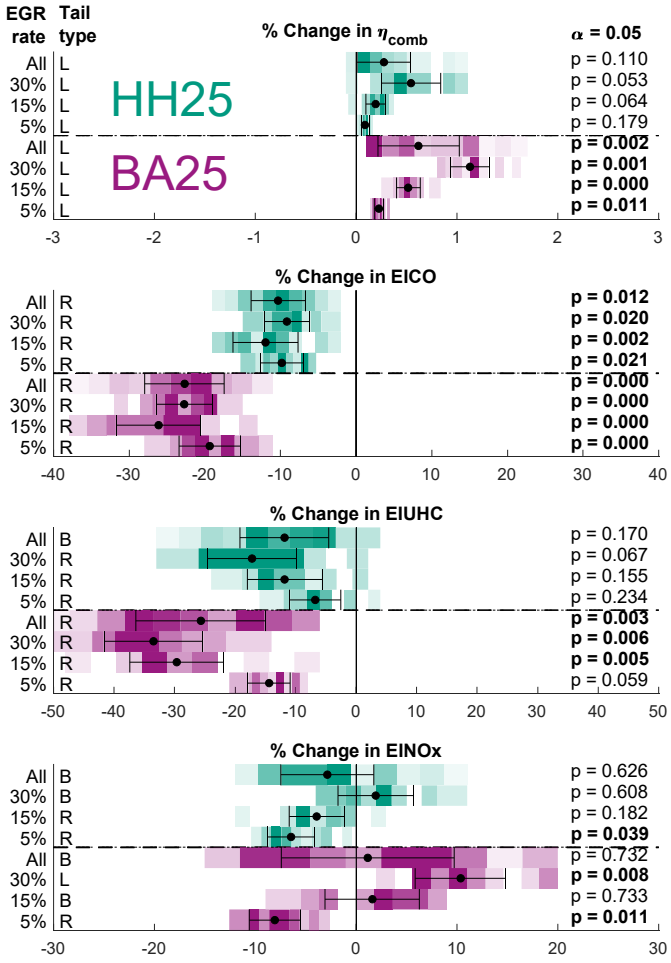

Figure 13: T-test evaluations of effects of oxygenate blends on exhaust emissions. Each plot shows the change in a parameter relative to the values obtained with certification diesel. The colored bars are used to indicate the distribution of values for each EGR rate and overall for both HH25 (teal) and BA25 (purple). The black dots represent the mean value of the relative differences and the black lines indicate the standard deviation of the relative differences.

While evidence that HH25 increases combustion efficiency is limited, BA25 very likely increases combustion efficiency. Both oxygenates decrease CO emissions and do so most effectively at 15% EGR. BA25 is more effective at reducing CO emissions than HH25, which is consistent with BA25's higher reactivity and the earlier heat-release phasing it promotes. Mean data suggest that HH25 may reduce UHC emissions to an extent that increases with EGR. As with CO, BA25 more effectively reduces UHC emissions, but it does so more effectively as EGR rate increases. HH25 likely reduces NO_x emissions at 5% EGR, but there is no strong evidence to suggest it does so at higher EGR rates. Bulk gas temperature behavior (not shown) is not consistent with this reduction in NO_x emissions at 5% EGR, so it is not possible to explain this observation with the data available. BA25 results in a reduction in NO_x emissions at 5% EGR, no discernable effect at 15% EGR, and an increase in NO_x emissions at 30% EGR. BA25 significantly enhances pilot and main heat release at this most dilute condition (see Figure 10), so the observed increase in NO_x emissions is consistent with the increase in bulk-gas temperatures resulting from earlier, more robust pilot and main heat-release events.

The effects of the oxygenate blends on tradeoffs between exhaust temperature, UHC/CO emissions, and the degree of constant volume combustion are shown in Figure 14. Given the scatter in exhaust temperature data with the certification diesel fuel and the data shown in Figure 12, no conclusions can be drawn about the effect of the oxygenates on the tradeoff between DCVC and exhaust temperature. Similarly, there isn't compelling evidence to suggest that these oxygenated fuels improve the tradeoff between UHC emissions and combustion phasing. However, the significant improvement in CO emissions through the use of these oxygenates does appear to improve the CO-DCVC tradeoff, particularly at the lowest CO emissions levels.

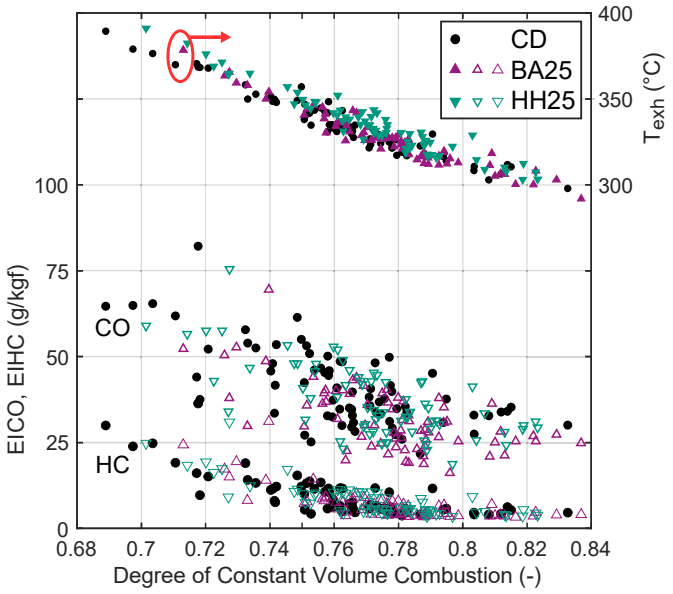

Figure 14: The effect of fuel oxygenate blends on exhaust temperature, CO, and UHC emissions plotted against DCVC. CD: black diamonds; BA25: purple triangles; HH25: teal triangles.

Fuel reactivity effects

Fuel reactivity effects have been studied by doping the certification diesel fuel with varying proportions of di-tert-butyl peroxide (DTBP). The effect on measured exhaust temperatures and the evolution of bulk gas temperatures are shown for the hottest-exhaust calibration in Figure 15; recall that the only differences in injection strategy are slight changes to main injection duration needed to maintain load. As with the EGR variation, the trend in bulk gas temperatures at 120 CAD ATDC matches the trend in measured exhaust temperatures. For this EGR rate and calibration, increasing fuel reactivity decreases exhaust temperature. While the addition of DTBP has a significant effect on bulk gas temperatures before 20 CAD ATDC, bulk gas temperatures are largely independent of fuel reactivity between 20 and 40 CAD ATDC. The behavior after 40 CAD ATDC is entirely responsible for the differences in bulk gas temperature at the end of the cycle, and is therefore likely responsible for the observed behavior in exhaust gas temperatures.

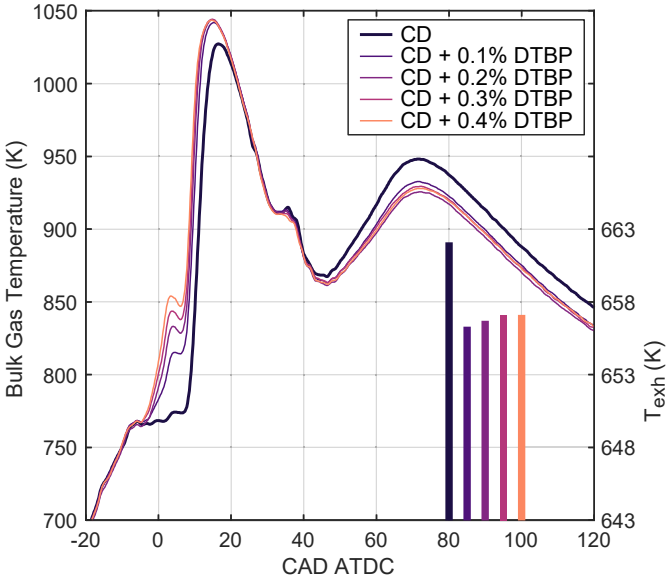

Figure 15: Bulk gas temperature plotted against crank angle for the hottest-exhaust calibration with 30% EGR and fuel reactivity as a parameter. Measured exhaust temperatures are shown with bar plots but the horizontal locations of the bars have no significance.

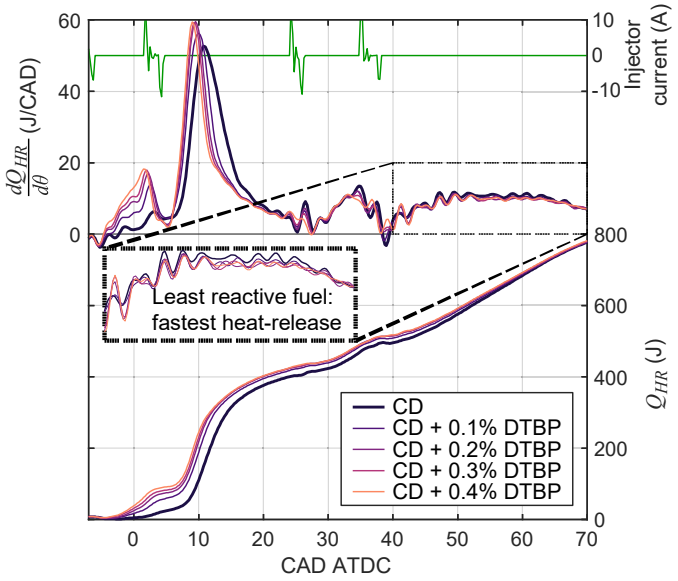

Figure 16: Injection current, heat-release rate, and cumulative heat release plotted against crank angle for the hottest-exhaust calibration with 30% EGR and fuel reactivity as a parameter.

Heat-release behavior during this late portion of the cycle determines the sensitivity of exhaust temperatures to fuel reactivity. The heat-release rate and cumulative heat release are shown for the hottest-exhaust calibration with 30% EGR in Figure 16. Fuel reactivity has a predictable effect on the heat-release associated with the pilot and main heat-release: it promotes robust pilot heat release, advances main heat release, and increases peak heat-release rates, albeit with diminishing returns as the concentration of DTBP increases. However, the effects on the heat-release associated with the post injections are more subtle and demonstrate that increasing fuel reactivity does not enhance heat-release of post injection mixtures. This behavior is best seen in the cumulative heat-release curves. At the end of the heat release event associated with the main injection (near 25 CAD ATDC), the cumulative heat released with the un-doped CD fuel is lower than for the doped fuels. The difference in cumulative heat release between doped and un-doped fuel at 25 CAD ATDC is nearly 6%, which is greater than the difference in total fueling of 1% or less. This means the pilot and main fuel have reacted to a lesser extent with certification diesel fuel than with the more reactive doped fuels. This difference essentially disappears by 70 CAD ATDC because slightly higher heat release rates are observed with the CD fuel during this phase, particularly those associated with the second post injection (see detail box in Figure 16). These higher heat-release rates are counterintuitive: they cannot be explained by the lower reactivity of the CD fuel. Rather, this behavior is consistent with the delayed reaction of pilot and main fuel that did not react before 25 CAD ATDC. This extra amount of late-stage heat release distinguishes the heat-release behavior of the un-doped CD fuel from that of all of the doped fuels and reduces the value of DCVC by approximately 2% for the CD fuel compared to all others. The more complete combustion of the pilot and main fuel is likely the reason for the decrease in exhaust temperatures observed with the doped fuels.

At the 5% EGR rate, the effects of fuel reactivity on measured exhaust temperatures are typically different than the observations at 30% EGR, although late-cycle behavior is still very important. Bulk gas temperatures and measured exhaust temperatures are shown in Figure 17 for the third injection strategy calibration shown in Figure 3. Measured exhaust temperatures first decrease as fuel reactivity increases, but then increase with continued increases in fuel reactivity. This behavior is observed to a much smaller extent for the 30% EGR case than for the 5% EGR case. The trend in bulk gas temperatures at 120 CAD ATDC matches this behavior to a lesser extent than it did for the 30% EGR case, but bulk gas temperatures do match the overall decrease-then-increase of temperatures as fuel reactivity increases. The ordering of late-cycle bulk gas temperatures is determined by the in-cylinder phenomena that occur after approximately 30 CAD ATDC.

Figure 18 shows the heat-release behavior for the 5%-EGR calibration that produced the temperature trends seen in Figure 17 for the baseline CD fuel, the CD fuel doped with 0.1 vol% DTBP, and the CD fuel doped with 0.4 vol% DTBP. Fuel reactivity has a clear impact on the pilot heat-release, but the differences in integrated heat release become very small during the main heat-release event. Both the un-doped CD and the most reactive doped fuel show slightly enhanced reactivity during short portions of the heat-release event associated with the second post injection. This behavior is not observed for any of the intermediate doped fuels; neither this enhanced late-cycle heat-release nor the reasons for its absence with the intermediate doped fuels are well understood. As with the 30% EGR case, the increased late-cycle reactivity may be attributed to the delayed reaction of some of the pilot/main mixture, although this effect is more subtle at 5% EGR than what was observed at 30% EGR. The cylinder pressure filter cutoff frequency does affect the pressure oscillations observed during combustion, but the filtering is applied consistently to all data. Changes in pressure filtering ultimately do not change the mechanism proposed in this work to explain the trends in measured exhaust temperatures with changing fuel reactivity.

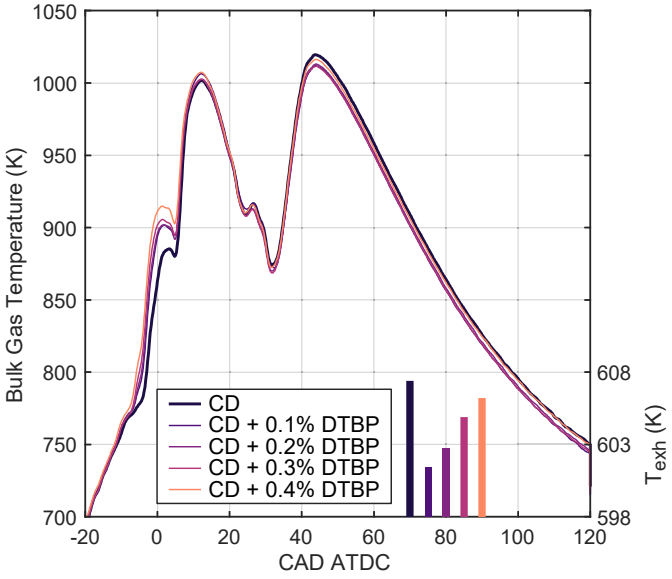

Figure 17: Bulk gas temperature plotted against crank angle for a 5% EGR case with fuel reactivity as a parameter. Measured exhaust temperatures are shown with bar plots but the horizontal locations of the bars have no significance.

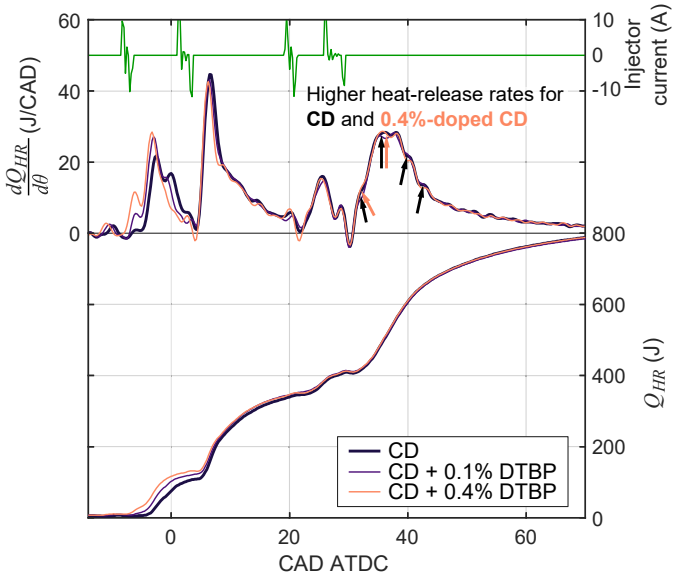

Figure 18: Injection current, heat-release rate, and cumulative heat release plotted against crank angle for a 5% EGR calibration and fuel reactivity as a parameter. The differences in heat-release behavior are more subtle than the ones observed at 30% EGR.

While some of the effects of fuel reactivity on pollutant emissions are expected, others are not. These effects are summarized in terms of relative changes compared to un-doped CD fuel in Figure 19. Increasing fuel reactivity above that of the certification diesel improves combustion efficiency, but there is no evidence that increasing the concentration of DTBP above 0.1% further increases combustion efficiency. However, the reduction in CO emissions observed with DTBP doping scales with DTBP concentration, with diminishing returns. The strongest evidence that DTBP doping can reduce UHC emissions is seen for the lowest doping level, but this conclusion cannot be made for any of the other doping levels. This unexpected result remains poorly understood, and does not suggest that more reactive fuels enable later combustion behavior to achieve hotter exhaust temperatures for a fixed UHC level. This appears to contradict the findings of Kurtz and Polonowski, who show that diesel fuels with higher cetane ratings can enable optimized calibrations with later combustion phasing, higher exhaust temperatures, and reduced UHC emissions [1]. Finally, the increase in NOx emissions with doping appears consistent with more robust, advanced heat-release, but it is relatively insensitive to doping level. The reduction in CO emissions and the increase in NOx emissions are consistent with the low-load results shown by Kurtz and Polonowski [1]. Further study and analysis will be necessary to resolve the discrepancy in the UHC/exhaust temperature tradeoffs.

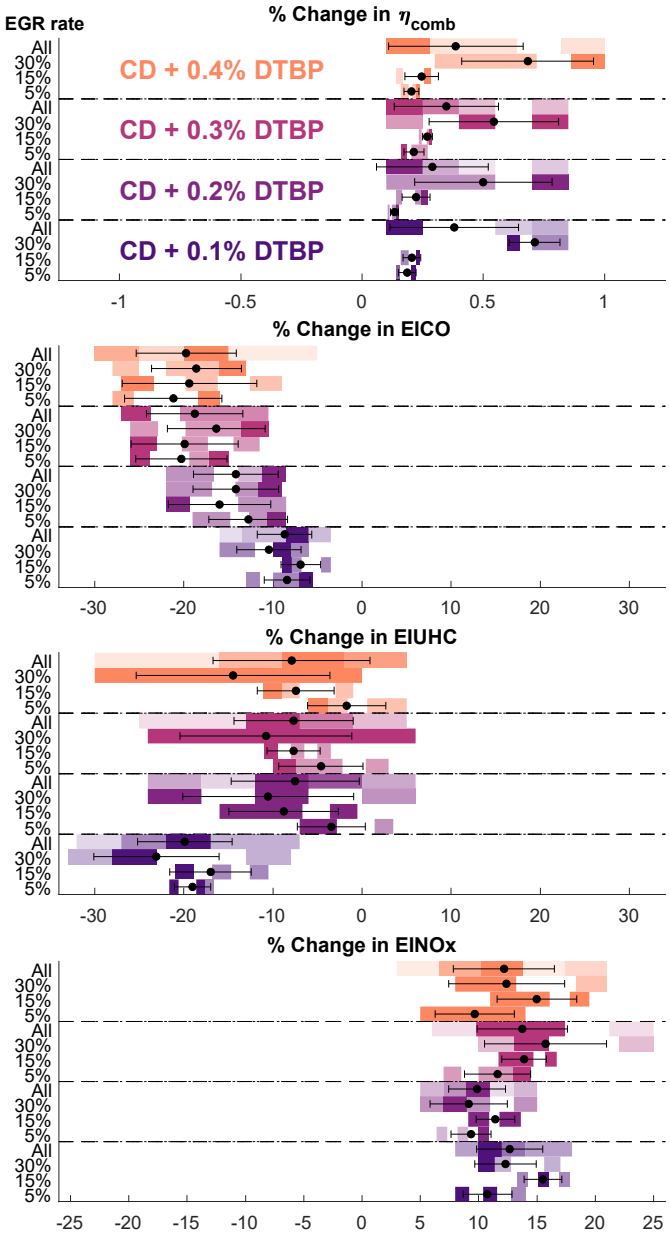

Figure 19: A summary of the effects of fuel reactivity on combustion efficiency, CO emissions, UHC emissions, and NOx emissions. The reference fuel is un-doped certification diesel (CD).

It is noted that both the more reactive BA25 oxygenate blend and the DTBP-doped certification diesel fuel resulted in decreased exhaust temperatures, particularly at 30% EGR. The mechanisms for these reductions both appear to be related to late-cycle behavior: the more reactive fuels result in slightly lower heat-release rates during the heat-release associated with the post injections. However, the manifestation of this effect is different for the oxygenated blends than for the DTBP-doped fuels. Heat-release appears to stop sooner for the oxygenated blends than for the certification diesel fuels (Figure 10). In contrast, heat-release rates are slightly lower for the more reactive doped fuels than for the certification diesel, but the duration of heat release is not changed to a significant extent (Figure 16). Very close inspection of the data shown in Figure 10 suggests that oxygenates may actually slightly increase peak heat-release rates during the combustion of the post injection. It is unclear why the more reactive BA25 blend does not decrease heat-release rates associated with the combustion of post injections in the same way that the DTBP-doped fuels do. One likely possibility is that the chemical kinetics pathways that govern the delayed reaction of pilot/main mixture are affected differently by the presence of DTBP than by the presence butylal. Improved understanding of this behavior through numerical simulations of this behavior will be necessary to provide guidance on fuel properties that may benefit or at least maintain catalyst-heating performance, or to help determine if such an effect can be robust enough to enhance catalyst-heating operation in real-world scenarios. Numerical simulation of this phenomenon will be a challenge: it will require very accurate prediction of mixing and chemical reactions over a period of several milliseconds, during which temperatures and pressures vary dramatically. Future experimental efforts will provide information about the origins of hydrocarbons found in the exhaust. When combined with variations of fuel cetane number, this approach is expected to provide further insight into the mechanisms by which fuel reactivity can influence both exhaust emissions and exhaust temperatures.

Summary/Conclusions

In this work, an experimental technique was developed and applied to study a five-injection catalyst heating operating strategy in a medium-duty diesel research engine. Thermodynamic analyses and exhaust emissions measurements have been used to provide insight into the effects of EGR rate, injection strategy calibration, oxygenate blending, and fuel reactivity on tradeoffs inherent in catalyst-heating performance. Hexyl hexanoate and butylal are studied as 25 vol% blends with certification diesel fuel. Certification diesel fuel is also progressively doped with di-tert-butyl peroxide to vary its reactivity. The key conclusions of this work are as follows:

1. EGR decreases DCVC and therefore increases exhaust temperatures, but at the expense of decreased combustion efficiency and exhaust enthalpy flow (Figures 4 and 5).
2. The behavior responsible for the hottest-exhaust calibrations and for many of the fuel property effects on exhaust temperature occur late during the cycle, when the heat-release associated with the post-injection mixtures takes place (Figures 7, 8, 10, 11, 15, 16, 17, and 18).
3. Oxygenate blends require higher injected masses because of their reduced lower heating value but advance combustion phasing and increase wall heat losses; the balance of these effects can negatively impact exhaust enthalpy (Figure 12).
4. Oxygenate blends improve combustion efficiency but can increase NOx emissions relative to baseline operation with certification diesel (Figure 13).
5. Increasing fuel reactivity can decrease exhaust temperature by enhancing the combustion of the pilot and main mixtures and reducing their propensity to react later in the cycle, particularly at high EGR rates when pilot combustion is poor (Figure 15 and Figure 16).
6. Higher fuel reactivity results in higher combustion efficiency, lower CO emissions, and higher NOx emissions (Figure 19); this is consistent with the literature.
7. The methodology applied in this work does not provide support for findings in the literature demonstrating that increasing fuel cetane rating enables injection strategy calibrations with hotter exhaust and reduced pollutant emissions.

References

1. California Air Resources Board, “Heavy-Duty Engine and Vehicle Omnibus Regulation and Associated Amendments”. Accessed 2/13/2021: https://ww2.arb.ca.gov/es/rulemaking/2020/hdomnibuslownox
2. Kurtz, E. and Polonowski, C. J., "The Influence of Fuel Cetane Number on Catalyst Light-Off Operation in a Modern Diesel Engine." SAE International Journal of Fuels and Lubricants 10(3), 2017.
3. Mercuri, D., Pozzi, C., Natì, G., Cassani, S., "Multi-After Injection Strategy to Optimize Exhaust Gases Temperature and Combustion Stability in Diesel Engine," presented at 24th Aachen Colloquium Automobile and Engine Technology, Aachen, Germany, October 5-7, 2015.
4. Neely, G. D., Sharp, C. and Rao, S., "CARB Low NOx Stage 3 Program - Modified Engine Calibration and Hardware Evaluations." SAE Technical Paper 2020-01-0318, 2020, DOI: https://doi.org/10.4271/2020-01-0318.
5. Fioroni, G., Fouts, L., Luecke, J., Vardon, D., Huq, N., Christensen, E., Huo, X., Alleman, T., McCormick, R., Kass, M., Polikarpov, E., Kukkadapu, G. and Whitesides, R. A., "Screening of Potential Biomass-Derived Streams as Fuel Blendstocks for Mixing Controlled Compression Ignition Combustion." SAE International Journal of Advances and Current Practices in Mobility 1(3): 1117-1138, 2019, DOI: https://doi.org/10.4271/2019-01-0570.
6. Deraad, S., Fulton, B., Gryglak, A., Hallgren, B., Hudson, A., Ives, D., Morgan, P., Styron, J., Waszczenko, E. and Cattermole, I., "The New Ford 6.7L V-8 Turbocharged Diesel Engine." SAE Technical Paper 2010-01-1101, 2010, DOI: https://doi.org/10.4271/2010-01-1101.
7. Somhorst, J., Oevermann, M., Bovo, M. and Denbratt, I., "A Method to Evaluate the Compression Ratio in IC Engines with Porous Thermal Barrier Coatings." SAE Technical Paper 2018-01-1778, 2018, DOI: https://doi.org/10.4271/2018-01-1778.
8. MacCalman, A.D., 2013. “Flexible Space-Filling Designs for Complex System Simulations”, PhD Thesis, Naval Postgraduate School, Monterey. http://hdl.handle.net/10945/34701
9. MacCalman, A.D., 2012. DesignCreatorv2 spreadsheet. Available online: http://harvest.nps.edu [accessed 6/17/2020].
10. Mueller, C. J., "The Quantification of Mixture Stoichiometry When Fuel Molecules Contain Oxidizer Elements or Oxidizer Molecules Contain Fuel Elements." SAE Technical Paper 2005-01-3705, 2005, DOI: https://doi.org/10.4271/2005-01-3705.
11. Co-Optimization of Fuels & Engines: Fuel Properties Database. Available online: www.nrel.gov/transportation/fuels-properties-database [accessed 2/1/2021].
12. Goodrich, B. E., McDuff, P. J., Krupa, C. C., Alvarez, L., Williams, A. M. and DeJovine, J. M., "A No-Harm Test Matrix Investigating the Effect of Di-tert-butyl Peroxide (DTBP)

Cetane Number Improver on Diesel Fuel Properties." SAE Technical Paper 982574, 1998, DOI: https://doi.org/10.4271/982574.
13. Woschni, G., "A Universally Applicable Equation for the Instantaneous Heat Transfer Coefficient in the Internal Combustion Engine." SAE Technical Paper 670931, 1967, DOI: https://doi.org/10.4271/670931.
14. Heywood, J. B. (1988). Internal Combustion Engine Fundamentals. New York, McGraw-Hill.
15. Dernotte, J., Dec, J. E. and Ji, C., "Energy Distribution Analysis in Boosted HCCI-like / LTGC Engines - Understanding the Trade-Offs to Maximize the Thermal Efficiency." SAE Int. J. Engines 8(3): 956-980, 2015, DOI: 10.4271/2015-01-0824.
16. Shudo, T. and Nabetani, S., "Analysis of Degree of Constant Volume and Cooling Loss in a Hydrogen Fuelled SI Engine." SAE Technical Paper 2001-01-3561, 2001, DOI: 10.4271/2001-01-3561.
17. Musculus, M. P. B., Miles, P. C. and Pickett, L. M. (2013). "Conceptual models for partially premixed low-temperature diesel combustion." Progress in Energy and Combustion Science 39(2): 246-283. DOI: https://doi.org/10.1016/j.pecs.2012.09.001.

Contact Information

Stephen Busch
sbusch@sandia.gov

Acknowledgments

Eric Kurtz and Chris Polonowski (Ford Motor Company) are gratefully acknowledged for their guidance in the development of the experimental approach and for productive discussions of the results. Tim Gilbertson and Kent Smith (Sandia National Laboratories) are thanked for technical support during the design, fabrication, and commissioning of the medium-duty diesel research engine. Christopher Nilsen and Julien Manin are acknowledged for their insightful reviews of this manuscript.

Part of this research was conducted as part of the Co-Optimization of Fuels & Engines (Co-Optima) project sponsored by the U.S. Department of Energy – Office of Energy Efficiency and Renewable Energy, Bioenergy Technologies and Vehicle Technologies Offices. Co-Optima is a collaborative project of several national laboratories initiated to simultaneously accelerate the introduction of affordable, scalable, and sustainable biofuels and high-efficiency, low-emission vehicle engines.

Sandia National Laboratories is a multimission laboratory managed and operated by National Technology and Engineering Solutions of Sandia, LLC., a wholly owned subsidiary of Honeywell International, Inc., for the U.S. Department of Energy's National Nuclear Security Administration under contract DE-NA-0003525. The views expressed in the article do not necessarily represent the views of the U.S. Department of Energy or the United States Government.

Definitions/Abbreviations

BA	Butylal, or dibutoxymethane
BA25	Blend of 25 vol% butylal in certification diesel fuel
CAD	Crank angle degrees
CAD ATDC	Crank angle degrees after top-dead center
CD	Certification diesel fuel
CO	Carbon monoxide
CO2	Carbon dioxide
DC	Direct current
DCVC	Degree of constant volume combustion
DOE	Duration of energizing
DTBP	Di-tert-butyl peroxide
EGR	Exhaust gas recirculation
EICO	Emissions index for CO
EIHC	Emissions index for UHCs
EINO$_x$	Emissions index for NO$_x$
HH	Hexyl hexanoate
HH25	Blend of 25 vol% hexyl hexanoate in certification diesel fuel
IMEP, IMEP$_n$	Indicated mean effective pressure, net indicated mean effective pressure
ISFCn	Net indicated specific fuel consumption
LVDT	Linear variable differential transformer
N$_2$	Molecular nitrogen
NO$_x$	Oxides of nitrogen
O$_2$	Molecular oxygen
SCR	Selective catalytic reduction
SOE	Start of energizing

TDC	Top-dead center
UHC	Unburned hydrocarbons
A_{cyl}	Instantaneous combustion chamber surface area
α	Threshold value for t-test
b	Constant in Woschni heat transfer correlation
B	Bore diameter
C_1	Motored velocity scale factor in Woschni heat transfer correlation
C_2	Combustion-induced velocity scaling factor in Woschni heat transfer correlation
C_m	Woschni tuning parameter
$c_{p,exh}$	Constant-pressure specific heat of exhaust gas
γ	Ratio of specific heats
ΔT	Temperature difference between exhaust gas and ambient
η_{th}	Thermal efficiency
η_{comb}	Combustion efficiency
η_{Otto}	Ideal Otto-cycle efficiency
$h_{Woschni}$	Convective heat transfer coefficient according to Woschni's correlation
$\dot{m}_{air}$	Mass flow rate of intake air not associated with simulated EGR
$\dot{m}_{exhaust}$	Mass flow rate of exhaust
m_{fuel}	Mass of fuel per cycle
$\dot{m}_{fuel}$	Mass flow rate of fuel
n	Engine speed
P	Fired cylinder pressure
P_{mot}	Motored cylinder pressure
Φ_{ex}	Exhaust heat flux
Q_{HR}	Heat release (cumulative)
Q_{LHV}	Lower heating value of fuel
$Q_{LHV,CO}$	Lower heating value of CO
Q_{wall}	Wall heat loss (cumulative)
r_c	Compression ratio
R_s	Swirl ratio
T_{cyl}	Bulk gas temperature
T_{wall}	Wall temperature
θ	Crank angle
S	Stroke
v_{mp}	Mean piston speed
V	Instantaneous cylinder volume
V_c	Clearance volume
V_d	Engine displacement volume
W_i	Indicated work
y_{CO}	Mass fraction of CO
y_{UHC}	Mass fraction of unburned hydrocarbons in exhaust